Molecular insights into the mechanisms of humidity-induced changes on the bulk performance of model castor oil derived polyurethane adhesives

Latchmi C. Raghunanan[a,*], Susana Fernandez-Prieto[b], Inmaculada Martínez[a], Concepción Valencia[a], M. Carmen Sánchez[a], and José M. Franco[a,*]

[a] *Departamento de Ingeniería Química, Facultad de Ciencias Experimentales, Universidad de Huelva, Campus de El Carmen, Huelva 21071, Spain.*

[b] *Procter & Gamble, Temselaan 100, 1853 Strombeek Bever (Belgium)*

**Corresponding Author: Fax: 34-959-219983; Tel: 34-959-219995; E-mail: franco@uhu.es*

Abstract

This work advances the development and use of sustainable polyurethane elastomers as green adhesives by providing insights into the mechanisms of humidity-induced changes on adhesive performance. Using a model adhesive prepared from equimolar ratios of castor oil and hexamethylene diisocyanate under facile reaction conditions, we show that the subtle changes in the chemical composition which occur with curing under different humidity environments significantly impact the cohesive integrity of the adhesives and, thus, their performances with different systems. The curing chemistry was evaluated based on the isocyanate consumption, which was followed using Fourier Transform Infrared Spectroscopy and Differential Scanning Calorimetry. Thermal, mechanical and adhesion properties were evaluated from thermogravimetric analysis, differential scanning calorimetry, rheology, tacking and lap shear tests. Moisture-cured adhesives were less covalently crosslinked, harder, more resistant to deformation, and recovered faster upon shear deformation compared to those cured otherwise. These mechanical properties complimented adhesive lap shear performance with substrates which formed covalent bonds during curing. For substrates with which covalent bonds could not form during curing, however, decreased internal cohesive integrity and associated increased hardness by urea formation resulted in poorer adhesive lap shear performance. This is contrary better tack performances obtained for the moisture-cured adhesives, attributed to their increased polarity and the energy dissipating ability.

Keywords: Adhesive; Castor oil; Urethane; Moisture curing; Humidity; Rheology.

1 Introduction

Despite the need to increase the environmental sustainability involved in the production of industrial and end-use materials, the incorporation of renewable feedstock into such processes continues to be a major hurdle. This is the result of many factors including the cost of the raw materials, technology changes necessary to incorporate different feedstock and/or processing routes, and the performance of materials produced from renewable feedstock compared to the well-established products already in the marketplace [1]. Obviously, improving the performance of renewably-derived materials is one part of the collective solution to widen their incorporation into the marketplace.

Bio-based polyurethanes possess the potential to make a significant impact in the marketplace. This is evident from the numerous literature which exist on the use of renewable feedstock for the production of polyurethane materials such as foams, rigid plastics, flexible hard plastics, elastomers, sealants, coatings and adhesives [2-5]. The most common means of preparing polyurethanes, and the one most employed commercially, involves the reaction of polyisocyanates with polyols [6]. Based on the structure and functionality of the raw materials and the conditions of the experiment, polyurethanes with different properties can be prepared. For example, the formation of rigid polyurethanes are generally favoured when aromatic isocyanates [7] and/or high NCO/OH molar ratios [8-10] and/or polyols with high OH functionality [8-10] are used. On the other hand, elastomeric urethanes are favoured by aliphatic isocyanates [7], with the incorporation of dangling chains in the soft polyol segments [10], and/or at lower NCO/OH molar ratios [8-10].

Castor oil is a naturally occurring polyol, making it one of the more preferred renewable feedstocks for polyurethane syntheses [2, 11]. Unlike other vegetable oils, the fatty acid profile of castor oil is relatively unchanged regardless of where or when the crop is harvested [12], a homogeneity desirable for manufacturing purposes [2]. Furthermore, while

its relatively low functionality (~ 2.7 OH/triglyceride) makes it suitable for the direct production of soft flexible polyurethanes and the like [2], polymer rigidity and mechanical properties can be improved by suitable functionalization of the reactive ester groups of the triglyceride backbone and/or at the many carbon-carbon double bonds of the unsaturated fatty acid moieties (which account for over 98% of the composition of castor oil) [2, 12]. Thus, castor oil can be used directly as a natural polyol in the syntheses of polyurethanes [13-16], or it may be suitably modified prior to the formation of polyurethanes [6, 17-19].

At the Chemical Product and Process Technology Center (Pro^{2}TecS, Universidad de Huelva), we have restricted our efforts to only those technologies which employ castor oil directly as a reactive raw material – without further functionalization -, and thus, which benefit from improved atom efficiency, simplicity and, therefore, more sustainable product engineering [20-23]. Our efforts have recently contributed to the patenting of biobased polyurethane gels and adhesives prepared from castor oil and isocyanates using a facile solvent free protocol [24, 25]. These polyurethanes can retain high loadings of hydrophobic materials, are transparent, and are readily formed into complex shapes, making them suitable for home and air care applications [25]. Another desirable property of gels and adhesives for these applications is resistivity to changes in humidity. For instance, humidity can vary from 30 -100 % on any given day in urban coastal areas [26], can reach as low as < 15 % in countries which experience harsh winters [27], and is typically set to 50-65 % rH in air conditioned environments [28]. The moisture-curing ability of isocyanate-containing urethanes, however, are well known [29]. Moreover, the resulting compositional changes upon moisture-curing may lead to differences in mechanical and adhesive properties that can impact the overall performance properties either positively or negatively [30-32].

We expect that castor oil-derived polyurethanes with tunable-on-demand properties tailored to our applications can be prepared if we are able to predict the changes in material

properties which occur upon curing at different humidities. In Daniel-da-Silva *et. al* [33], FTIR and DSC were used to follow the curing kinetics of NCO-terminated urethanes at 55 % rH. Based on the hydrogen bonding evolution, they showed the increasing tendency of the urea moieties toward phase separation with increasing free NCO content. Phase separation, in turn, leads to improved elasticity and tensile strength [34] – desirable properties in adhesives. However, Madhour and Azzam [34] also reported that tear strength – another important parameter in adhesives – decreases with increased phase separation. Most recently, Ling *et. al.* [35] used FT-NIR to measure the formation of urea and urethane during the *in-situ* curing reaction (at 23 °C and 50 % rH) of an aqueous isocyanate-containing adhesive sandwiched between two paper substrates. In Chattopadhyay *et. al.* [36], the evolution of chemical crosslinking during the curing reaction at 25 °C and 45-50 % rH was studied using DMTA. The same group also reported improved adhesive strengths for bulk systems which possessed higher degrees of phase separation [37]. Ren and Frazier [38, 39], however, observed that despite obvious changes to the bulk adhesive properties and the adhesive-substrate bondline and penetration with hard segment content (curing at room temperature, 65 % rH), adhesive-substrate fracture was insensitive to hard segment content. This was attributed to a switch from a dual-phase morphology to a continuous hard phase above a certain critical hard segment content. Overall, these works all reinforce the ongoing need to study and correlate the chemical composition of NCO-containing adhesives with their performance properties. However, it is also apparent from these summaries that all of the humidity-dependent works reported in the literature thus far have been restricted to curing at ~50 % rH – *i.e.*, at near ambient humidity. To date, only one work can be found in the literature describing the evolution of chemistry with curing for a given NCO-containing polyurethane system at different curing humidities (15, 45, 75 % rH) [40], and even then this work does not extend to correlations with performance properties.

In this contribution, therefore, we have employed spectroscopic, calorimetric and rheological time-dependent studies to correlate the curing processes and structural evolution of a model castor oil-derived polyurethane adhesive to changes in its chemical composition during curing under different humidity environments. We expect that the insights gained from this work will contribute to the larger body of knowledge that informs on the intelligent design of sustainable bio-derived adhesives with increased durability against environmental damages due to humidity. The formulation, comprised of castor oil and hexamethylene diisocyanate (HMDI), was selected so that the resulting adhesive would be NCO-terminated, thus giving strong adhesion with H-active surfaces via the formation of covalent urethane links. The curing chemistry of the selected adhesive was determined from Fourier transform infrared (FTIR) and differential scanning calorimetry (DSC) experiments. The resulting changes in the thermal and mechanical properties during curing were followed using thermogravimetric analysis (TGA), differential scanning calorimetry (DSC), and rheological measurements. Final adhesion performance properties were evaluated from tacking and lap shear experiments.

2 Materials and Methods

2.1 Materials

1,6-hexamethylene diisocyanate (HMDI, 98.0% purity), tetrahydrofuran (GPC grade), xylene (reagent grade), lithium chloride (LiCl, ≥ 99 % purity), magnesium nitrate ($Mg(NO_3)_2$, ≥ 99 % purity) and barium chloride ($BaCl_2$, ≥ 99 % purity) were purchased from Sigma-Aldrich. Castor oil (211 cSt at 40 °C) was obtained from Guinama (Spain). All materials were used as received without further purification.

2.2 Synthesis of adhesives

Castor oil (84 parts by weight) and HMDI (16 parts by weight) were combined, covered, and stirred at 200-300 rpm at room temperature for 24 hours to give the desired adhesive formulation. The nomenclature of the obtained formulation and its molar compositions are presented in Table 1.

Table 1: Summary of adhesive composition.

Formulation nomenclature	8416
Weight ratio (castor oil: HMDI)	84:16
Mole ratio (castor oil: HMDI)*	1:1.05
Mole ratio (OH:NCO)*	3:2.1
Isocyanate index (NCO:OH)	0.70

*based on an idealized composition of 100% ricinolein for castor oil.

2.3 Curing studies

Except for the tacking and lap shear experiments, which were performed on the fully cured adhesives, all other experiments were performed as a function of curing time. Cure progression was monitored via the consumption of the isocyanates as determined from FTIR experiments such that the fully cured systems were free of isocyanates. All characterization measurements were performed on samples obtained from at least three independent reactions. Upon completion of each reaction (*i.e.*, at time zero; *t0*), the adhesives were transferred into suitable molds, as noted below (see also Figure S.1 in the Supporting Information), and allowed to cure under different relative humidities (rH). For the FTIR, ^{1}H-NMR, GPC and TGA measurements, the samples were cured on polypropylene discs (1 mm thickness; 2 mm diameter). For the DSC measurements, the samples were cured directly in the hermatic aluminum pans typical of DSC experiments and sealed only at the time of the actual measurement. For the rheology experiments, samples were also cured directly on disposable plate-plate geometries. Finally, samples for the tacking experiments were cured on baked

silica sheets (2 mm thickness) cut to the desired specification (35 mm diameter for stainless steel substrates and 20 mm for wood substrates).

Humidity control during curing was achieved using suitable saturated salt solutions in sealed chambers as follows: LiCl, $Mg(NO_3)_2$ and $BaCl_2$ for 11, 54 and 90% rH, respectively [41-43]. The saturated salt solutions were prepared by dissolving the respective salts in distilled water at room temperature. In each instance, excess salt was piled into a cone at the center of the chamber and the system was allowed to equilibrate before use. At equilibrium, the relative humidity within each chamber would be determined by the affinity of the respective salt for water; *i.e.*, salts which consumed more water for dissolution retained more water in the liquid phase, resulting in a lower humidity of the gaseous phase and vice versa. Where specified, adhesives were also cured under uncontrolled ambient conditions by leaving the systems open to the atmosphere in an air-conditioned room set to 25 °C.

NCO-containing samples for ^{1}H-NMR and GPC measurements were first dissolved in excess methanol to quench any unreacted isocyanate (Scheme S.1 in the Supporting Information). Methanol was subsequently removed by evaporation at room temperature followed by drying under vacuum at room temperature for 24 hours.

2.4 Characterization

2.4.1 Fourier Transform Infra-Red (FTIR)

Fourier Transform Infra-Red (FTIR) measurements were performed using a Jasco FT4200 infrared spectrometer (JASCO Inc., Tokyo, Japan) equipped with an attenuated total reflectance (ATR) system. Samples were loaded onto the ATR crystal area and the respective spectra obtained in the transmission mode over a scanning range of 4000–400 cm^{-1} for ~ 80 repeated scans at a resolution of 4 cm^{-1}. All spectra were transformed into the absorbance

mode using the Spectra Manager software (version 2.10.2.1), baseline corrected and normalized to the CH_2 peak area.

2.4.2 Nuclear Magnetic Resonance (^{1}H-NMR)

^{1}H spectra were acquired on a Bruker Avance 500 MHz spectrometer (Bruker, USA) equipped with a 5-mm Broadband Observe (BBFO) probe with z gradient. Spectra were acquired at 25 ºC over a 16- ppm spectral window with a 10 s recycle delay, 32 transients. Spectra were Fourier transformed, phase corrected, and baseline corrected. The spectral width was 10330.572 Hz for ^{1}H. Chemical shifts were referenced using tetramethyl silane as internal reference and $CDCl_3$ ($\delta(^1H)$ = 7.24 ppm) as solvent. Spectra were analysed using ACD/NMR Processor Academic Edition software (Version 12.01).

2.4.3 TGA

Thermogravimetric Analysis (TGA) measurements were performed using a Q50 model TGA (TA Instruments, New Castle, DE, USA) under constant nitrogen flow (sample flow 60 mL/min; balance flow 40 mL/min). Typically, 12-17 mg of sample were loaded onto a platinum pan and heated to 600 °C at a rate of 10 °C/min. TGA data were analysed using the 'TA Universal Analysis' software (Version 4.5A).

2.4.4 DSC

DSC measurements were carried out on a Q100 model (TA Instruments, New Castle, DE, USA) under a nitrogen flow of 50 mL/min. Typically, the adhesive (6.5 ± 1.0 mg) in a hermetically sealed aluminum pan was equilibrated at -80 °C for 5 min and then heated to 250 °C at 10 °C/min to give the curing profile (first cycle). Where required, subsequent cooling and heating at the same temperature limits and temperature ramps were performed to give the consecutive cooling and heating thermograms. The data were analysed using the 'TA Universal Analysis' software (Version 4.5A).

2.4.5 Rheology

The viscoelastic behaviour of the adhesives at different cure times was investigated via small-amplitude oscillatory shear (SAOS) measurements inside the linear viscoelastic range (LVR) using a controlled-stress MARS rheometer (Thermo Haake, Germany) equipped with parallel plate-plate geometries (35 mm stainless steel and 20 mm disposable aluminium, depending on the adhesive cure time) and coupled to a thermostatic bath (Thermo, Germany). For each cure time reported, the LVR was first determined from stress sweep experiments performed between 0.01-1000 Pa at 25 °C with a fixed frequency of 1Hz (6.28 rad/s). Subsequent frequency sweep experiments were performed at 25 ºC in a frequency range of 100-0.3 rad/s, at a selected shear stress within the LVR as determined from the stress sweep experiments.

2.4.6 Probe tack

Tack tests were performed at 25 °C in tensile mode on a Shimadzu AGIS Universal Testing Machine (Japan) equipped with a 1 kN load cell and smooth plate-plate steel or wood geometries (35 mm and 20 mm diameters, respectively). Sample disks were loaded onto the bottom plate. The upper plate was lowered at a rate of 1 mm/s until a contact force of 1N was reached. This contact was maintained for 60 seconds following which the upper probe was removed at a rate of 1 mm/s. The required normal force for debonding was measured as a function of time. All measurements were performed in triplicate on new fully cured samples. For each system, adhesion energy (J/m^2) was calculated as the area beneath the experimentally obtained force-displacement (J) curve normalized to the surface area of the probe (m^2).

2.4.7 Lap shear

Lap shear experiments were performed using the Shimadzu AGIS Universal Testing Machine (Japan) on stainless steel (local supplier) and sycamore wood (local supplier) substrates according to modified versions of ASTM D1002 and D906, respectively. All of the substrates were cut according to the standard specifications. The stainless steel substrates were cleaned prior to use by washing with soap, distilled water, and acetone, in that order. The individually sealed wood substrates were used as obtained. No pre-conditioning was performed for any of the experiments.

For each experiment, a thin layer of freshly prepared adhesive (*i.e.*, at curing time = 0) was coated onto one end of the substrate using an applicator (18 × 18 × 0.5 mm^3 adhesive volume) and allowed to come into contact with another uncoated substrate under its own weight. The applicator was a flat stainless steel plate with a gap of 0.5 mm that was used to scrape off the excess adhesive from the substrate such that a fixed coating thickness of 0.5 mm was consistently obtained (Figure S.2 in the Supporting Information). All of the thus prepared substrates were allowed to fully cure under the specified curing humidity at room temperature. Lap shear strengths were subsequently obtained as the maximum load per square meter of shear area under a force ramp of 3.56 kN/min following the respective standard methods. The reported values were averaged from at least 5 experiments.

3 Results and Discussion

3.1 Synthesis

In this work, model biobased urethanes for use as adhesives were prepared by reacting castor oil with 1,6-hexamethylene diisocyanate (HMDI) under facile reaction conditions over 24 hours; *i.e.*, at room temperature, without using any solvent or catalyst, and without N_2

protection. The FTIR and ^{1}H-NMR spectra of the adhesive immediately following the reaction (*i.e.*, at curing time = 0 hrs, t_0) are presented in Figure 1 and Figure 2, respectively.

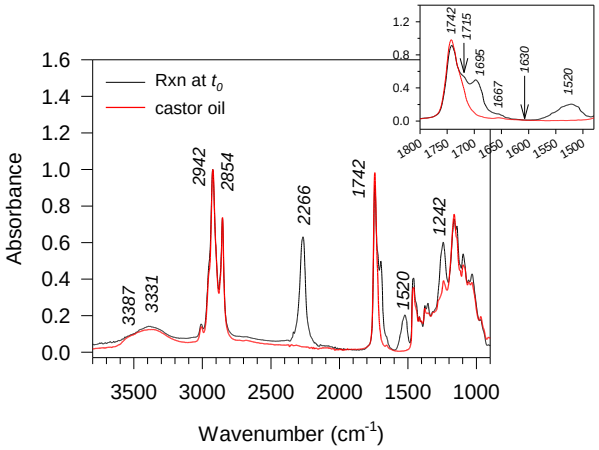

Figure 1: FTIR spectra of castor oil before and after reaction with HMDI for 24 hours. Characteristic wavenumbers are given, in cm^{-1}, above the respective absorbance peaks.

In Figure 1, the characteristic vibrations associated with castor oil include the aliphatic CH_2 asymmetric and symmetric stretching vibrations at 2854-2942 cm^{-1}, the broad OH peak at 3387 cm^{-1} (which can be further deconvoluted into the H-bonded and non-H bonded peaks at 3374 and 3523 cm^{-1}, respectively; results not presented), the ester C=O asymmetric stretch at 1742 cm^{-1}, and the *cis* C=C vibrations at 1667 cm^{-1}. The formation of urethanes at t_0 is evidenced by the appearance of the amide II band (C-N stretching + N-H bending) at 1520 cm^{-1}, and the free and H-bonded C=O amide I stretching vibrations at 1715 and 1695 cm^{-1}, respectively [44]. The increase in the signal at 1242 cm^{-1} and the shift in the peak at 3387 cm^{-1} to 3331 cm^{-1} are also consistent with the formation of urethanes; the former is due to the overlap of the amide III band (C-N stretching + N-H bending) with the deformation of the ester groups already present in castor oil, and the latter is due to the appearance of N-H bonds (3331 cm^{-1}) in the newly formed urethanes upon reaction of the alcohol with the isocyanate [44].

In the FTIR spectra of the adhesive at t_0, the isocyanate stretching vibration appears at 2266 cm^{-1}. The presence of this peak indicates that, at t_0, the isocyanate functional group was not fully reacted. This slow reaction rate of castor oil with HMDI is consistent with the kinetics of secondary alcohols with aliphatic isocyanates [45, 46], and is beneficial for the preparation of NCO-terminated pre-polymers that can form covalent bonds during the curing cycle with adherends containing surface active hydrogens. GPC experiments were used to confirm the absence of unreacted HMDI molecules in the adhesive at t_0 (Figure S.3 in the Supporting Information), indicating that all of the HMDI molecules were successfully crosslinked to castor oil to give the NCO-terminated pre-polymers.

Also of note from Figure 1 is the absence of the urea carbonyl peak at ~1630 cm^{-1} [44], revealing that the NCO-containing prepolymer obtained at t_0 is essentially free from urea. This indicates that, despite the known tendencies of isocyanates to react at least three times faster with water than with secondary alcohols [47], the facile reaction conditions employed for the synthesis of the biobased adhesive of this work were sufficient to favour the formation of urea-free polyurethane prepolymers.

The ^{1}H-NMR spectrum of the adhesive obtained at t_0 (Figure 2b) supports the results of the FTIR experiments. The aliphatic protons associated with the urethane group are apparent at 3.18 ppm (-O-(C=O)-NH-C$\underline{H}_2$), while those associated with the urea moiety are absent (C$\underline{H}_2$-NH-(C=O)-NH-C$\underline{H}_2$; δ 2.81). Note that the chemical shift at 2.7 ppm is present in the spectra of both the virgin castor oil and the adhesive at t_0 (Figures 2a and 2b, respectively), and cannot, therefore, be associated with the urea functional group. In fact, this peak is also observed in the ^{1}H-NMR spectra of castor oil normally found in the literature [9, 13], and may arise from naturally occurring impurities present in the castor oil itself.

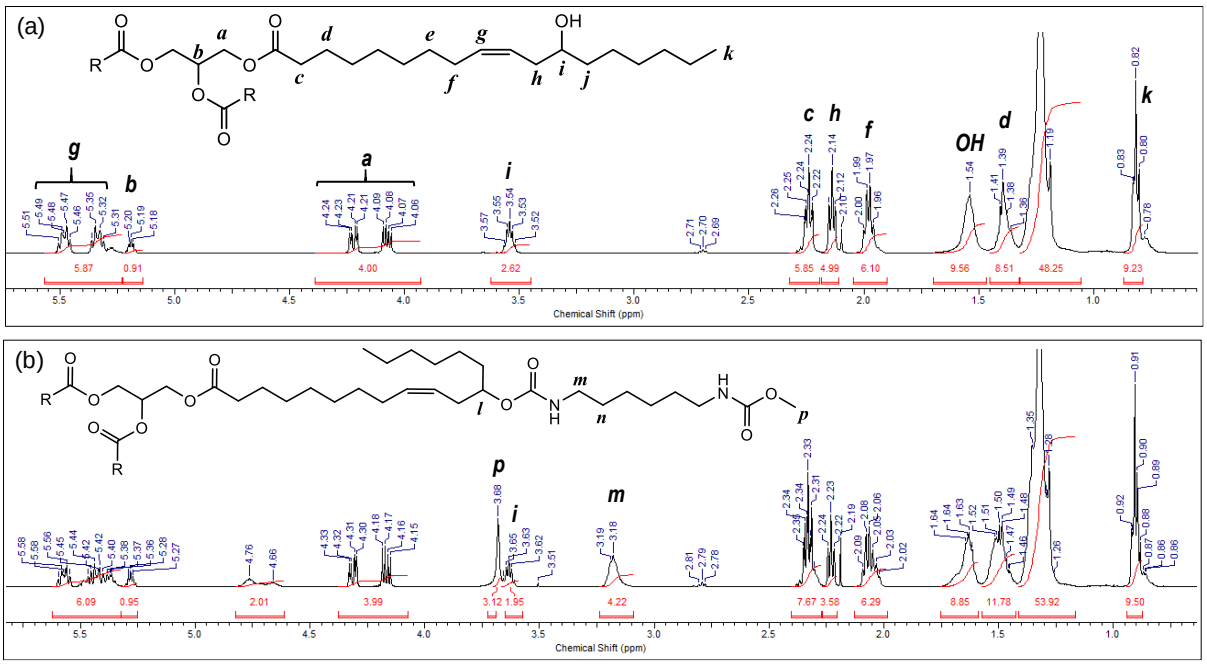

Figure 2: ^{1}H-NMR spectra (in $CDCl_3$) of (a) castor oil and (b) the methanol-quenched adhesive at t_0. The areas under the curves, equivalent to the number of protons, have been normalized to the CH_2 protons on the glycerol backbone of a single triglyceride molecule (protons labelled ***a*** in the spectra).

The ^{1}H-NMR spectra of castor oil (Figure 2a) shows that, for every one triglyceride molecule in castor oil, ~ 2.6 ricinoleic acid moieties are present (as given by the C<u>H</u>-OH protons; δ 3.52-3.57, 2.6H). After reaction with HMDI for 24 hours at room temperature (Figure 2b), the number of C<u>H</u>-OH protons decreases to ~ 2 per triglyceride molecule, indicating a 23% conversion of the available OH groups into urethanes. Considering further the proportion of methyl carbamates (C<u>H</u>$_3$-O-(C=O)-NH-; δ 3.68; 3H) in the methanol-quenched spectrum of the adhesive at t_0 (Figure 2b), the molar equivalent of isocyanates present at the end of the reaction can be determined; for every one methyl carbamate group formed, the equivalent of one NCO group would have been quenched (Scheme S.1, Supporting Information). Thus, from Figure 2b, it is apparent that at t_0, the excess NCO was just over 1 unit per triglyceride unit. Finally, since the peak area of the C<u>H</u>$_2$-NH-(C=O)-O-

protons (δ 3.18; 4H) gives the total urethanes formed from the reaction of NCO with both castor oil and upon quenching with methanol, we can deduce that for every one molecule of HMDI that reacted, only one urethane bond was formed with castor oil, such that the resulting triglyceride urethane at t_0 was NCO-terminated (Scheme 1). This result is consistent with the data of the FTIR and GPC experiments already presented.

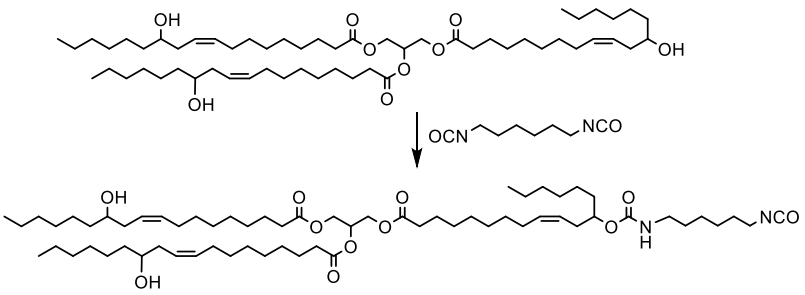

Scheme 1: Idealized synthesis of NCO-terminated polyurethane adhesives from castor oil and HMDI at room temperature.

Overall, these results show that urea-free NCO-terminated urethanes were successfully obtained under facile reaction conditions which included the absence of solvent, heat, catalyst and N_2 protection.

3.2 Curing Chemistry

Figure 3 shows the FTIR spectra of the model NCO-terminated urethane adhesive when fully cured in high and low humidity environments (*i.e.*, 90 and 11 % rH, respectively). Not surprisingly, two new vibrations appear at 1621 cm^{-1} and 1574 cm^{-1} in the spectrum of the adhesive cured at high humidity. These vibrations, associated with the urea carbonyl group (NH-(**C=O**)-NH) and the urea amide II band (C-N stretch and urea N-H bends), respectively, corroborate the formation of urea under the moisture-rich curing conditions [48]. The idealized curing reactions of the NCO-terminated urethane adhesive under the

different curing conditions are presented in Schemes 2a,b. Scheme 2c shows the detailed reactions of the NCO functional group to give urea in the presence of water.

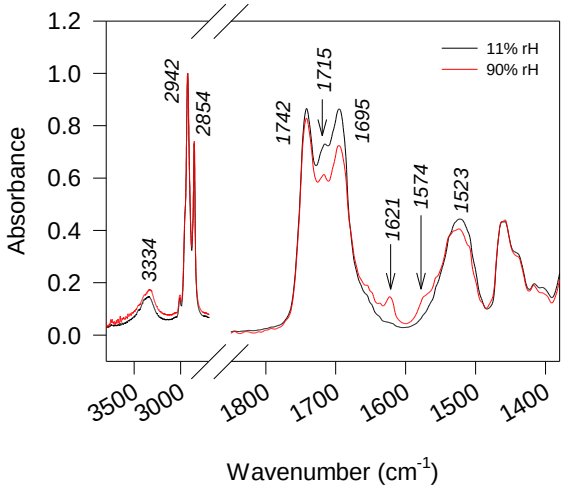

Figure 3: FTIR spectra of the fully cured adhesive (absence of NCO absorbance at 2266 cm^{-1}) subjected to different curing environments, *viz.* low and high humidities (11 and 90 % rH, respectively).

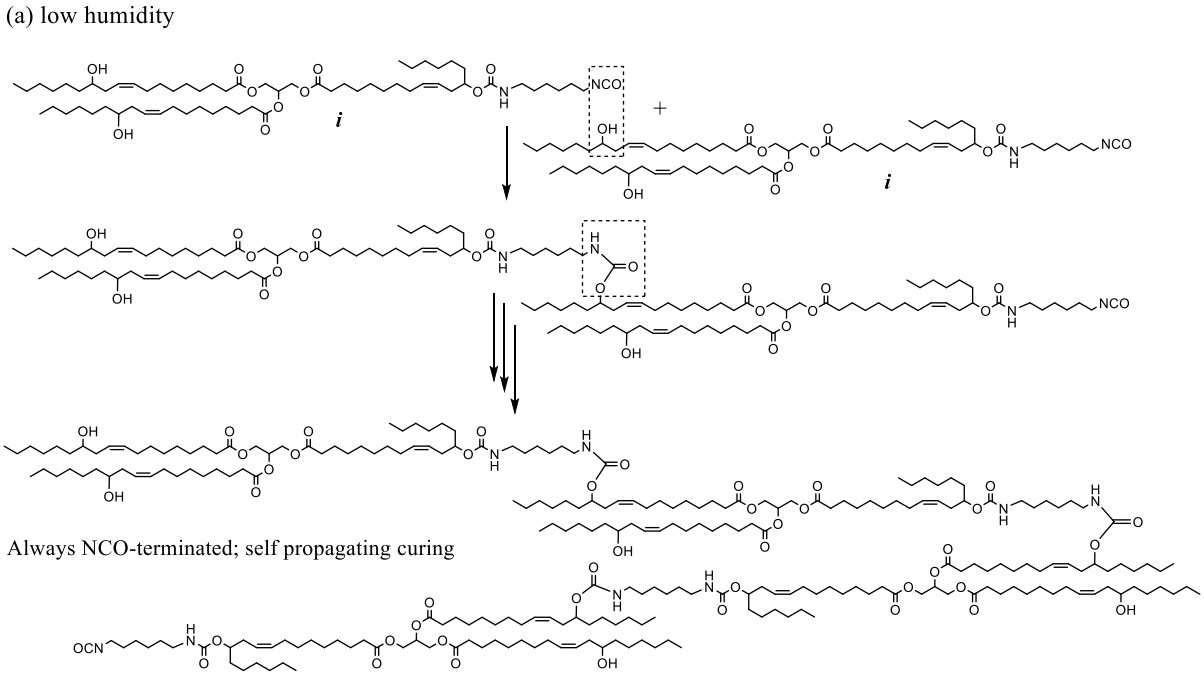

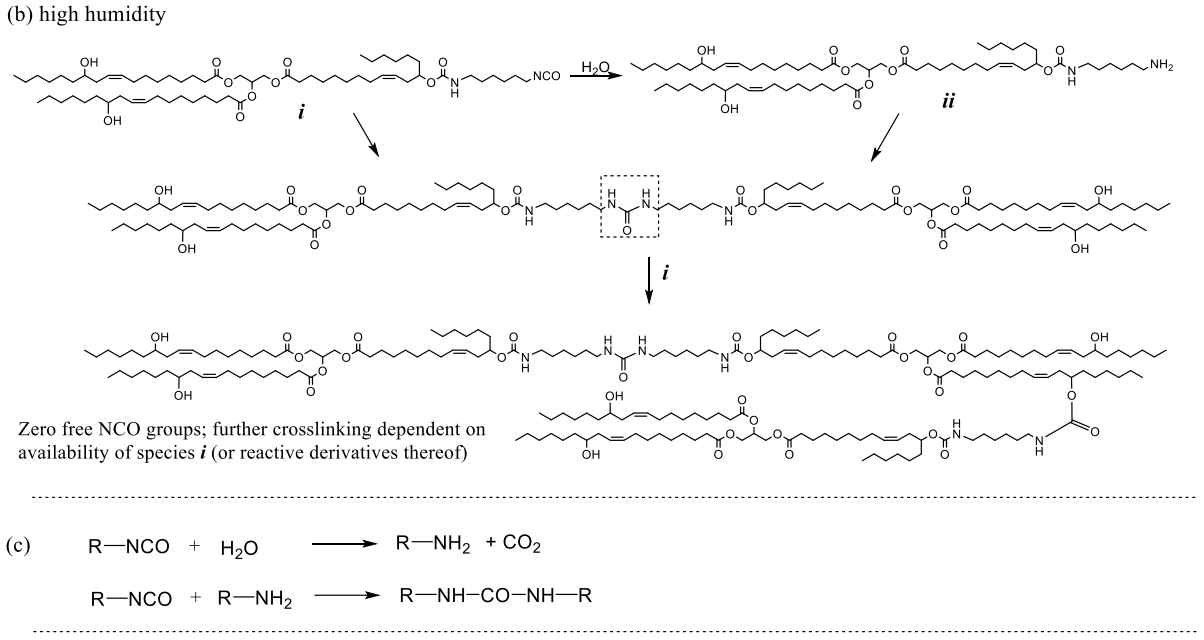

Scheme 2: Idealized curing of NCO-containing urethanes under (a) low and (b) high curing humidities; (c) typical reaction of isocyanates with water to give urea.

To understand further the changes in composition with time, the model NCO-terminated urethane adhesive was subjected to curing at four different humidities (low humidity, 11% rH; high humidity, 90% rH; controlled ambient humidity, 54% rH; and uncontrolled ambient humidity) and characterized at convenient intervals until fully cured using FTIR and DSC. From the FTIR experiments, available or unreacted NCO with time was determined from the areas associated with the NCO peak in the respective spectra. To account for the mass dependence of the absorbance signals in the FTIR experiments, each spectrum was normalized to the peak area of the unchanging aliphatic segments of the adhesives (*i.e.*, the CH_2 moieties at 2923 cm^{-1}). From the DSC experiments, the exothermic enthalpy derived from the first heating cycle (Figure 4) is associated with the temperature-promoted curing reactions of available NCO groups at time *t* (to give products such as urethanes, allophanates, biurets, etc [47, 49]), and is thus directly proportional to the available

NCO at time (*t*) [50, 51]. The normalized NCO peak areas and enthalpy values deduced from the FTIR and DSC analyses are presented in Figures 5a and 5b, respectively.

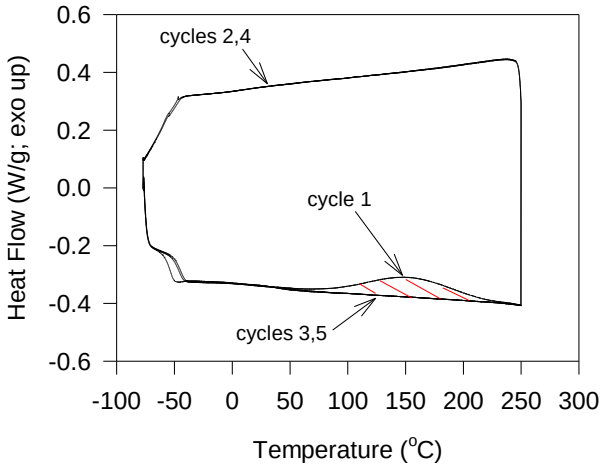

Figure 4: DSC heating (cycles 1, 3, 5) and cooling (cycles 2, 4) thermograms of an NCO-containing urethane adhesive showing the absence of crystallization and melting events. Shaded area shows enthalpy of curing reaction. Cooling and heating rates: 10 °C/min.

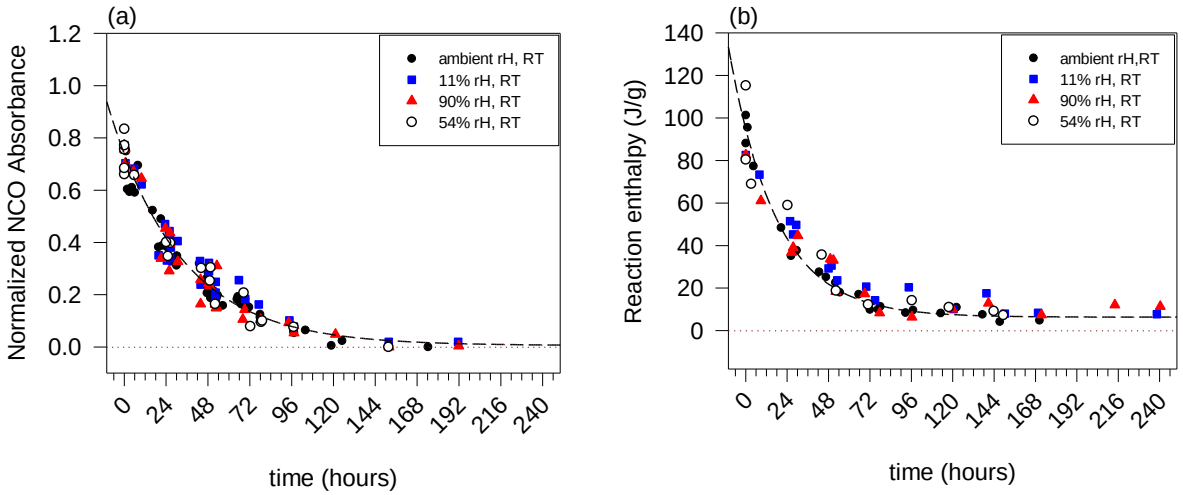

Figure 5: Influence of humidity on the curing kinetics of model NCO-terminate urethane adhesives as determined from (a) the normalized NCO peak areas of FTIR experiments, and (b) the area under the exothermic event in the first heating thermogram of the DSC experiments. Dashed lines are exponential fits of the NCO peak areas for experiments cured at uncontrolled ambient humidity.

Both Figures 5a and 5b show that, regardless of the curing conditions, the available NCO content decreased exponentially with time and, unexpectedly, the curing kinetics did not change with humidity. The latter is contrary to expected results since it is well established that the rate of NCO reaction with water is an order of a magnitude higher than it is with secondary alcohols [45, 49, 51, 52]. Furthermore, the curing reaction of isocyanates under high-moisture conditions consumes 2 molecules of NCO groups for every 1 molecule of H_2O that reacts (Scheme 2c). Combined with the already limiting amounts of reactive NCO groups in the adhesive formulation (Table 1), a difference in the rates of NCO consumption in the presence of moisture should have been observed. That these were not observed indicates the influence of some other factor on the curing kinetics.

Given that the influence of humidity on the curing chemistry of the adhesives was clearly apparent in Figure 3, we hypothesize that the influence of humidity on the kinetics is masked by mass transfer effects within the adhesive systems. As the curing reaction progresses, the increasing crosslinking density, molecular size and viscoelastic properties all contribute to decreased mobility of the NCO-containing molecules within the adhesive matrix. Thus, the continued formation of urea is increasingly dependent on the ability of the water molecules to diffuse within the adhesive matrix. This may be further impeded by the decreasing ability of the water molecules to diffuse from the atmosphere into the adhesive matrix due to the increasing thickness of the urea film formed closest to the air-adhesive interface [53].

In an effort to further elucidate the differences in the rates of the chemical reactions under different humidity, the regions of the FTIR spectra associated with the urea and urethane carbonyl stretching vibrations (*i.e.*, 1800-1600 cm^{-1}; Figure 6a) were deconvoluted. The results are presented in Figures 6b and 6c. Figure 6b shows the assignment of the vibrational peaks upon deconvolution of a typical spectra (wherein ‘bonded’ refers to the

hydrogen-bonded groups, and 'free' refers to those moieties which do not participate in hydrogen bonding interactions), and Figure 6c gives the relative crosslinking densities of the differently cured systems as a function of time (calculated as the areas associated with the urea and urethane carbonyl peaks normalized to the ester carbonyl peak of the castor oil component).

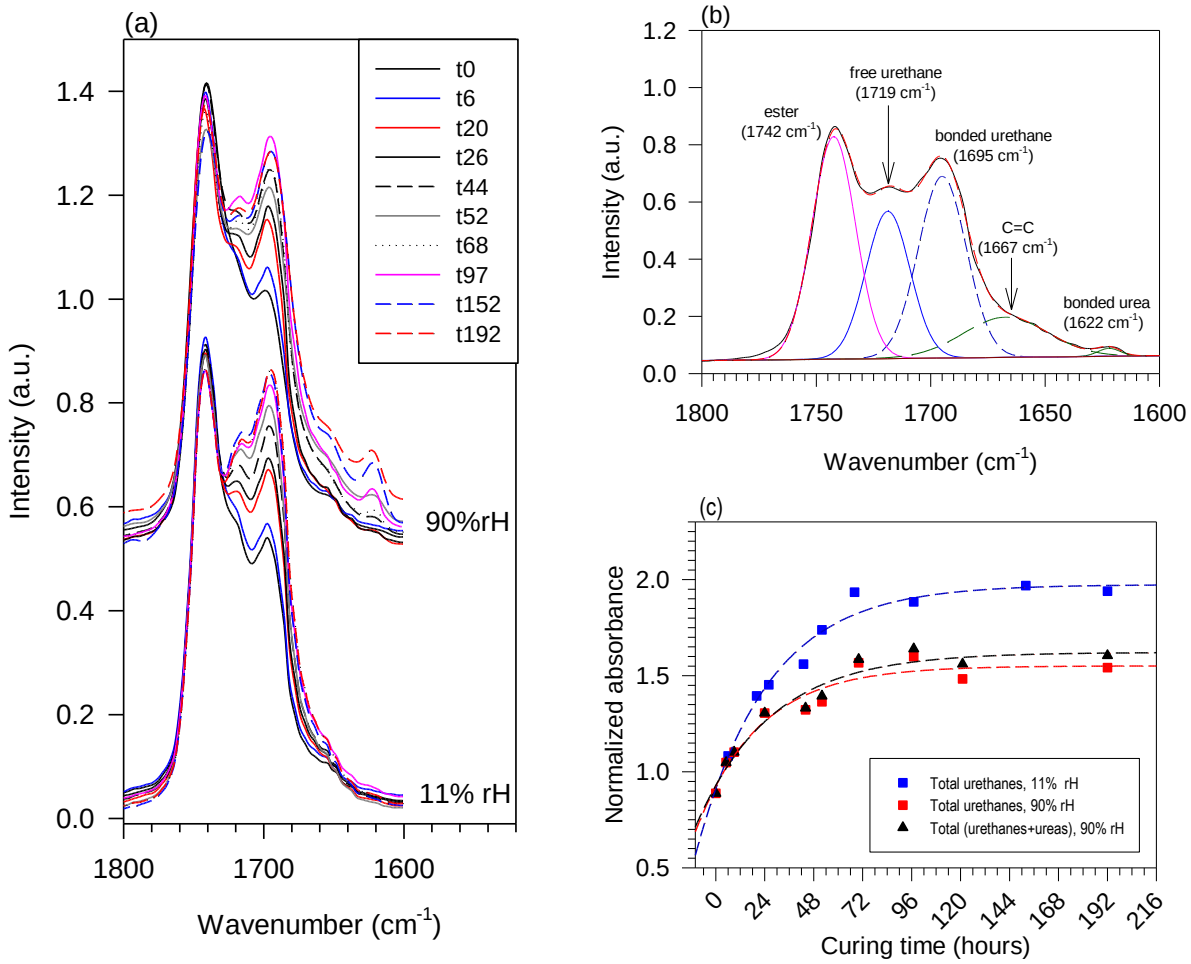

Figure 6: (a) Region of FTIR spectra containing C=O peaks associated with urethane and urea moieties in the differently cured adhesives; (b) typical deconvolution of a representative FTIR spectra showing the assignment of the C=O peaks in an adhesive cured at high humidity; (c) areas associated with urea and urethane carbonyl peaks, normalized to ester carbonyl peaks, showing the evolution of crosslinking density with cure progression.

As is apparent from Figure 6, no measurable urea was obtained at any cure time in the adhesive cured at low humidity. On the other hand, only the hydrogen bonded urea peak (1622 cm^{-1}) evolved with curing under the high humidity conditions; the peak associated with the free urea (1640 cm^{-1}) was absent at all cure times, indicating the preferred tendency of the urea moieties in these systems toward hydrogen bonding. Also apparent from Figure 6 is the small proportion of the urea compared to urethanes in these adhesives. In fact, it can be deduced from Figure 6c that the urea content formed under high humidity conditions accounted for less than 5% of the total crosslinking density of the fully cured adhesive (0.07 and 1.55 crosslink density of bonded urea and total urethanes, respectively of the 90% rH adhesive system). As we shall see in the subsequent sections, however, this amount was sufficient to result in significant changes to the materials properties of the resulting adhesives.

Figure 6c also shows that the total urethanes formed in the adhesive cured under low humidity conditions was greater than the sum of all of the urethanes and urea formed under high humidity curing conditions. That is, the adhesive cured at low humidity possessed higher crosslinking density compared to the adhesive cured at higher humidity. In fact, elucidation of the crosslinking densities of the final cured systems from Figure 6c reveals that the urea containing adhesive was ~ 20% less crosslinked than the urethane-only system (1.96 and 1.62 total crosslinking density for low and high humidity cured systems, respectively. At first, this result appears somewhat surprising. In hindsight, however, this should be expected; recall that for every one urea moiety that forms (*i.e.*, the equivalent of a single crosslink), two NCO groups must react (Scheme 2). This is in contrast with the formation of a urethane crosslink from every one NCO that reacts with an alcohol. In the urethane-only adhesive, therefore, for the same quantities of NCO consumed, a total of two crosslinks will be obtained for every one that forms from urea in the urea-containing systems.

Overall, these studies reveal that the curing humidity to which the NCO-terminated adhesives are subjected result in small but significant changes to chemical composition, affecting especially the crosslinking density of the material and, supposedly, its mechanical and/or adhesive properties.

3.3 Thermal and Mechanical Properties

3.3.1 Thermal Stability

The results of the thermal stability experiments are presented in Figure 7a-c. Specifically, Figure 7a shows the evolution of the TGA profiles with cure time for a representative adhesive (cured at 54% humidity); Figure 7b gives the TGA profiles of the fully cured adhesives obtained under the three different curing conditions (*i.e.*, 11, 54 and 90 % rH); and Figure 7c gives the associated DTG profiles of all of the differently cured adhesives at selected cure times. The onset of degradation (T_{ON}) and DTG peak temperatures have been listed in Table S.1 in the Supporting Information.

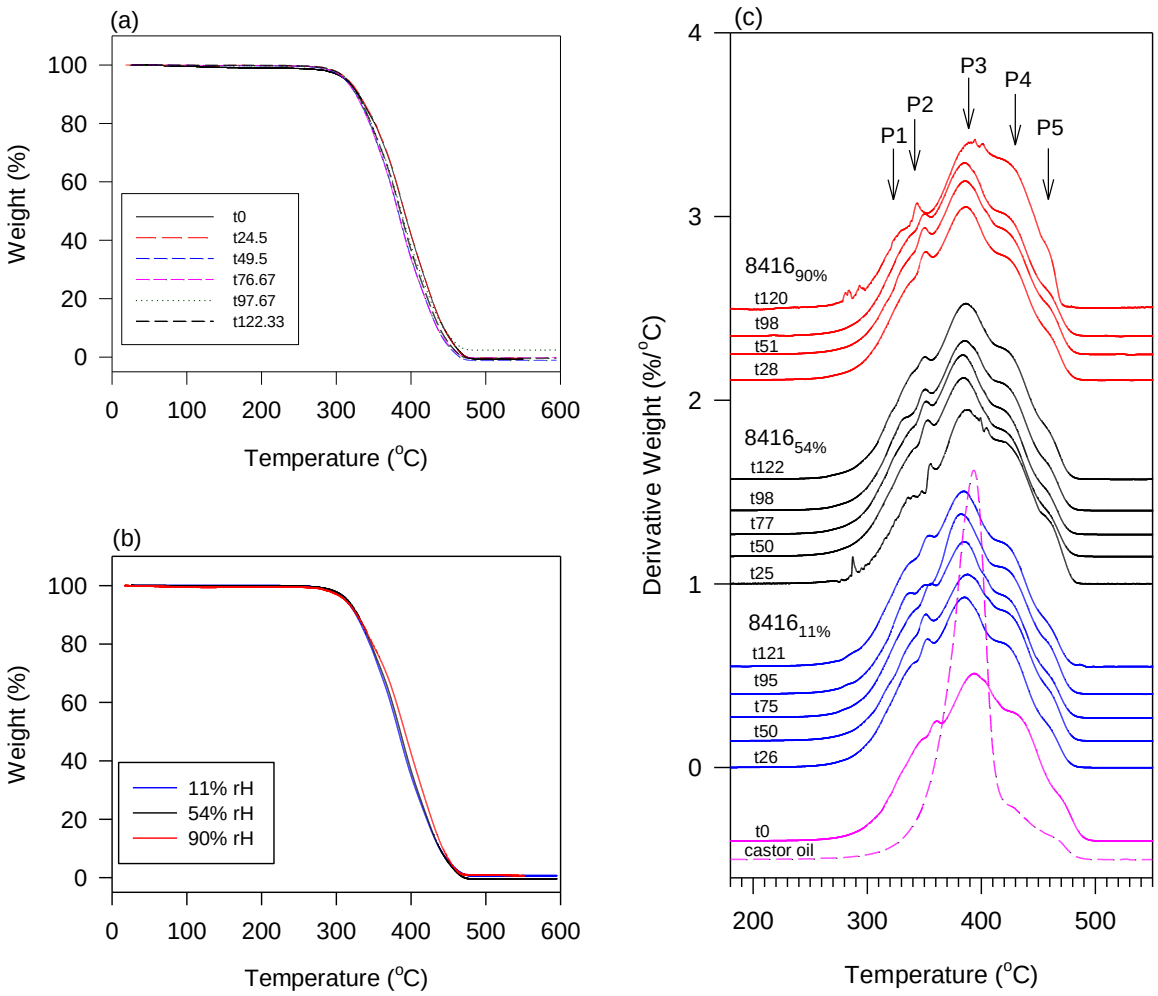

Figure 7: TGA profiles of (a) adhesive subjected to curing at 54% humidity conditions, taken at different curing times, and (b) fully cured adhesives obtained upon curing under different humidity conditions. (c) DTG profiles of differently cured adhesives at select curing times.

From Figure 7a, it is apparent that the thermal stability of the adhesive cured at 54% rH does not vary with cure time. Similar results were also observed with curing time for the adhesives obtained at lower and higher humidities (54% rH and 90% rH; results not presented). Further, Figure 7b shows that the thermal stability of the adhesives upon final curing is not changed by the humidity at which the systems are cured. In fact, from the DTG profiles presented in Figure 7c, it can be seen that all of the adhesives undergo thermal degradation between 285-480 °C via at least five closely occurring degradation steps whose peak temperatures (P1-P5) do not change significantly from adhesive to adhesive (Table S.1

and Figure S.4 in the Supporting Information). The similar thermal profiles can be explained by an *insitu* temperature promoted curing reaction between the unreacted NCO and castor oil (or other H-active species) during the early stages of the TGA experiments. Indeed, one might recall from Figure 4 that such a mechanism was in fact observed between 50-250 °C in the first heating cycles of the DSC experiments obtained under the same conditions as the TGA experiments (*i.e.*, heating rate 10 °C/min; N_2 atmosphere). This was further corroborated from simultaneous TGA-DTA experiments (results presented in Figure S.5 in Supporting Information) in which an exothermic peak assigned to the curing reaction was observed before 200 °C – well before the start of degradation based on TGA results alone, and which could not be a crystallization event based on the DSC results. Thus, these results demonstrate a high thermal stability of up to ~ 280 °C for all of the adhesives of this work - regardless of curing time -, revealing that the adhesives can be handled at all temperatures up to 280 °C during its life cycle. This high thermal stability is comparable to that of other vegetable oil-derived polyurethane adhesives [10] and analogous adhesives containing the glyceride backbone [54].

Figure 7c also shows that, unlike the adhesives, the thermal degradation of the unmodified castor oil occurs at a higher temperature (spanning 350-483 °C) and comprises of only three decomposition steps (P3-P5 in Figure 7c). This indicates that the first two decomposition events in the DTG profiles of the adhesives (P1, P2 in Figure 7c) are associated with the degradation of the urethane moieties, whilst the last three (P3-P5 in Figure 7c) are associated with the decomposition of the castor oil moieties.

Typically, the first stage in the inert atmosphere decomposition of vegetable oils involves the thermolysis of the triglyceride ester backbone to give the free fatty acids [55]. In castor oil, this step occurs between 351-413 °C and accounts for ~ 80% of the weight loss

observed (P3 in Figure 7c). At temperatures greater than 400 °C (P4 in Figure 7c), further decomposition of the fatty acid moieties results in secondary decomposition products such as heptaldeyde and undecenoic acid [12]. The last decomposition step (P5 in Figure 7c) is normally associated with the decomposition of residual carbonaceous content. From Table S.1 and Figure S.4 in the Supporting Information, it is apparent that the temperatures associated with the degradation of these castor oil moieties (*i.e.*, P3-P5) do not change significantly between the unmodified castor oil and the castor oil derived polyurethane adhesives, regardless of curing time or curing conditions.

Similarly, the onset of degradation and the peak DTG temperatures associated with the urethane moieties (P1 and P2 in Figure 7c) also do not change with curing time (Figure S.4 in the Supporting Information). As discussed above, this is the result of *in situ* curing during the progression of the TGA experiments. The decreased stability of the adhesives compared to the unmodified castor oil is also consistent with the lower thermal stability of urethanes [56]. This is due to the thermal susceptibility of the urethane bond itself, which undergoes thermolysis via N-H and/or C-H hydrogen transfer. The former results in depolymerization to regenerate the parent isocyanate and alcohol, while the latter gives typical decomposition products such as amines (primary and secondary amines from β- and α- C-H elimination, respectively), olefins and carbon dioxide, olefins [57-60].

3.3.2 Thermal Properties

A representative DSC showing the heating and cooling profiles over two consecutive cycles has already been presented in Figure 4. As can be seen, except for the glass transition temperature (T_g) and reaction enthalpies associated with the first heating cycle, the subsequent heating and cooling cycles were not affected by the thermal treatment; *i.e.*, the adhesives do not undergo any crystallization or melting events. This is true for all of the

adhesive systems, regardless of curing time or curing conditions. This behaviour, characteristic of highly amorphous strongly crosslinked systems [61], confirms that the polyurethane adhesives of this work were thermoset curing adhesives.

Since the first heating cycle is associated with the temperature-promoted curing of unreacted NCO (Section 3.2), it can be appreciated that the glass transition temperature is likewise associated with the thermal character of the adhesive at a given time *t* before its temperature promoted curing. In fact, the glass transition temperature represents the temperature below which a material goes from being rubbery to glassy, and will, therefore, be influenced by the amorphous content and crosslinked character of the adhesive at a given curing time [14, 61, 62]. This is shown in Figure 8 for the adhesive cured at two selected humidities, 90 and 11 % rH, which are representative of curing under high and low moisture environments, respectively.

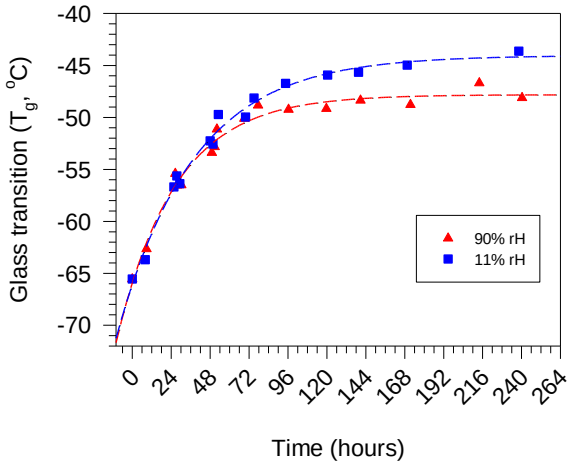

Figure 8: Evolution of the glass transition temperatures (obtained from the first heating cycle of the DSC experiments; 10 °C/min heating rate) of the adhesives during curing.

Figure 8 shows that the glass transition temperatures of the differently cured adhesives increased exponentially towards a maximum during curing at room temperature. For both systems, the T_g evolved in the same manner over the first three days of curing (~ 72

hours), after which the low humidity system continued to slowly increase towards a maximum of -44 °C whilst the high humidity system immediately plateaued at -48 °C. Note that this evolution is exactly analogous to the change in the total urethane and urea contents with curing time and humidity (*cf* Figure 6c, Section 3.2). This corroborates the strong influence of crosslinking on the thermal properties of the adhesives; as the network grows, the amorphous content becomes more easily immobilized and, thus, the glass transition occurs at higher temperatures. This result is also consistent with the known influence of hard segments on the glass transition temperature [61, 63].

3.3.3 Viscoelastic Behaviour

The values and evolution of the storage (G') and loss (G") moduli obtained from small amplitude oscillatory shear (SAOS) experiments were used to describe the viscoelastic properties of the adhesives. The experimentally obtained stress and frequency sweep curves are presented in Figures 9 and 10, respectively.

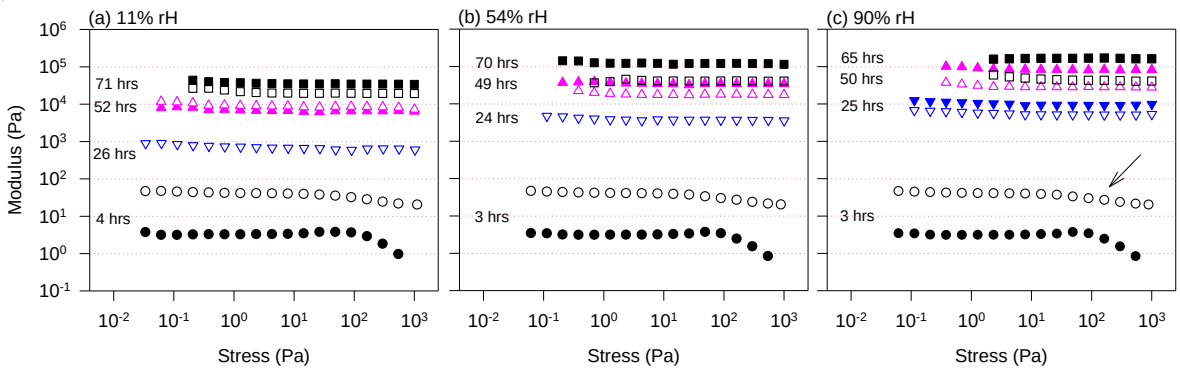

Figure 9: Stress-sweep curves of the adhesives taken at selected times during curing under different humidity conditions; (a) 11% rH, (b) 54% rH, (c) 90% rH. Curing time is listed alongside the associated curves. Open and closed symbols represent the viscous (G") and elastic (G') moduli, respectively.

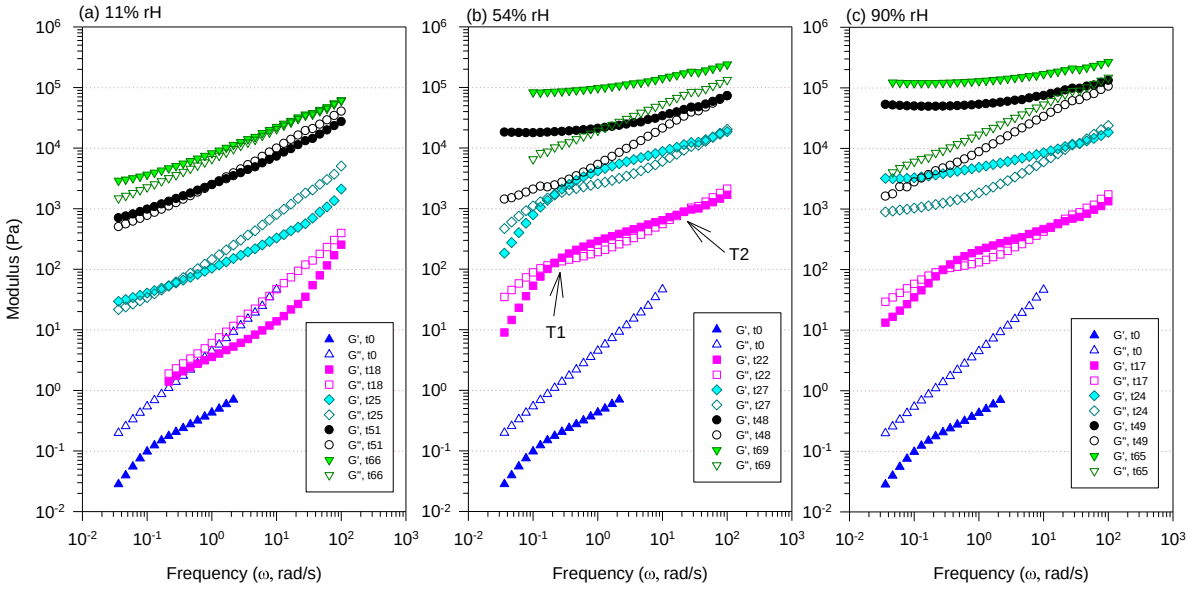

Figure 10: Frequency sweep curves of the adhesives taken at selected times during curing under different humidity conditions; (a) 11% rH, (b) 54% rH, (c) 90% rH. Open and closed symbols represent the viscous (G") and elastic (G') moduli, respectively; and T1 and T2 show the terminal-rubbery and rubber-glass transition crossover points, respectively.

As can be seen in Figure 9, a well extended LVR was obtained for all of the adhesives at all curing times, with the critical stress values for the onset of the non-linear regime always occurring higher than ~100 Pa (arrow in Figure 9c). Attending to the evolution of the SAOS functions with curing time, apart from a significant increase in both G' and G" with time, it is apparent that G" > G' for low curing times but G' > G" for the almost completely cured adhesives. Moreover, the time required to observe this crossover between both moduli is lower at high-humidity conditions. This effect is more clearly seen in the frequency sweep tests (Figure 10). Thus, for low humidity conditions (Figure 10a), G' ≈ G" after ~50h of curing, exhibiting an almost critical gel behaviour at this time. However, for the same curing time under higher humidity conditions, and especially for 90% rH, a well-developed plateau region – characteristic of highly entangled and/or crosslinked polymeric gels – with almost constant values of G' and a minimum value of G" at low frequencies is observed.

To better understand these results, their evolution with curing time have been summarized in Figure 11a-d. Figure 11a shows the progression of the elastic modulus (G') within the linear viscoelastic region (LVR) with time, Figure 11b gives the time-dependence of tan δ within the LVR (tan δ = G''/G', such that the material demonstrates a predominant fluid-like behaviour when tan δ > 1 and a solid-like behaviour when tan δ < 1), and Figures 11c and 11d gives the modulus and frequency, respectively, of the adhesives at the terminal-rubbery (T1) and rubber-glass transition (T2) crossover points (*i.e.*, when G'=G'').

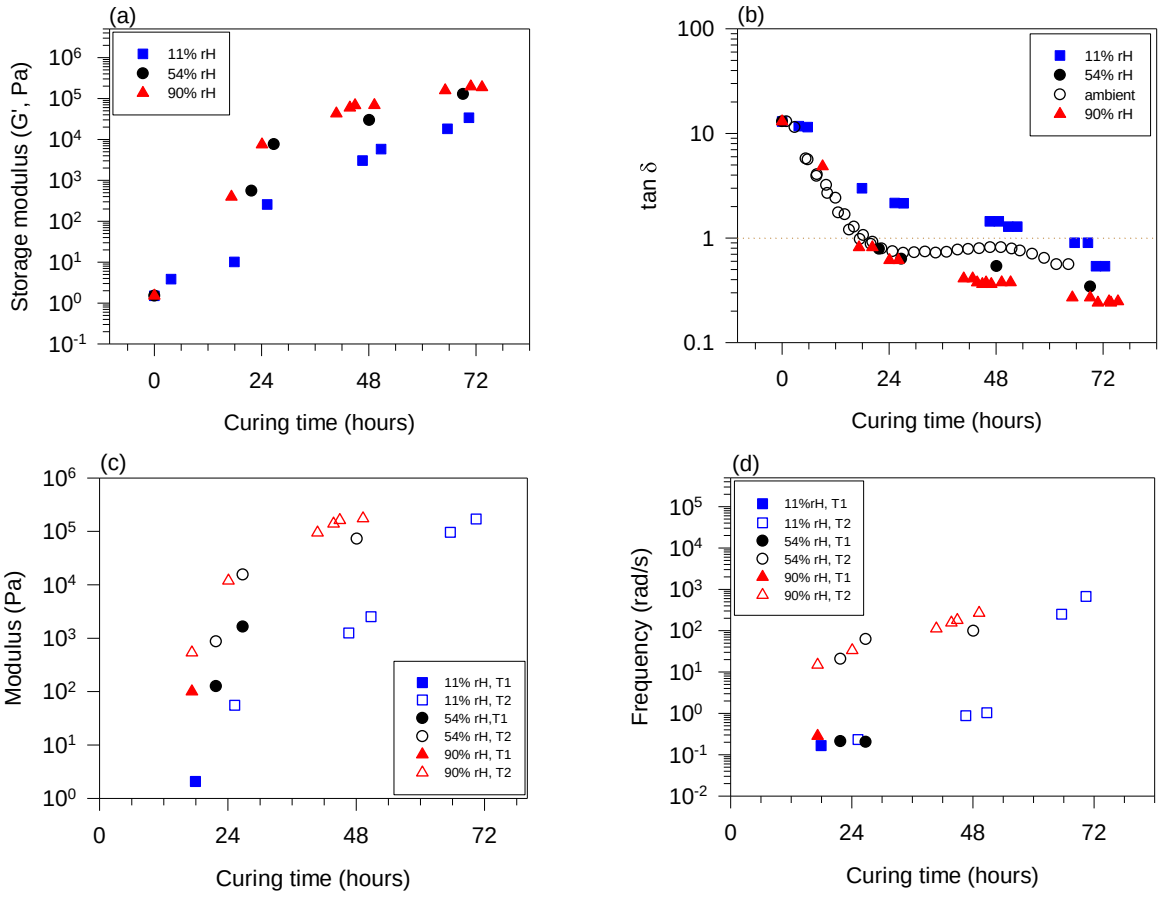

Figure 11. Influence of humidity on the rheology of PU adhesives. (a) Evolution of G' with time, at 1 Hz. (b) tan δ derived from frequency sweep curves at 1Hz (tan δ = G''/G'). (c) G' and G'' values at the crossover points and (d) crossover frequencies obtained from frequency sweep experiments (T1 and T2 refer to the terminal-rubbery and rubber-glass transition crossover points, respectively).

Figure 11a shows that the elastic moduli of the differently cured systems all increase with cure time, expectedly due to the increase in crosslinking with cure progression. In fact, the most significant changes in the moduli of the adhesives occur at the start of curing, increasing by up to 5 orders of magnitude over the first 3 days. This is in excellent agreement with the evolution of the crosslinking density of the adhesives (*cf* Figure 6c and Figure 5).

From Figure 11, however, it can also be inferred that crosslinking density is not the only factor influencing the rheology of the adhesives. Whilst the moduli – and in fact all of the associated rheological properties presented in Figure 11 - of the urea-containing adhesives are similar to each other, it is clearly apparent that, at any given time, the moduli of the adhesives cured at higher humidity are greater than that cured at low humidity. This indicates that the less crosslinked urea-containing adhesives are more resistant to deformation than the more crosslinked urethane-only adhesive. In fact, as previously mentioned, the adhesives cured at > 50% rH formed hard gels within the first 24 hours, while the adhesive cured at very low humidity (< 11% rH) was still a viscous liquid up to a curing time of ~50 hours. This can be especially appreciated from the tan δ values in Figure 11b. These observations, however, are contrary to the results already presented in Section 3.2 which show that the urea-containing systems are less crosslinked than the urethane-only adhesive; *i.e.*, the more deformation resistant systems (higher moduli) are not those with the higher crosslinking densities. Finally, Figure 11d shows that the rubber-glass transition (T2) crossover points are shifted to lower frequencies in the low humidity systems. This indicates longer characteristic relaxation times for the more crosslinked systems; *i.e.*, longer times to reform bonds following shear, which is associated with its lower resistance (lower moduli) to shear deformation compared to the harder urea-containing systems. Note that less marked differences in the crossover frequencies were observed at the terminal-rubbery (T1) transition for all of the adhesives.

Undoubtedly, the mechanical response of the gels cured at higher humidity is attributed to their urea content. The extensive plateau region found in the mechanical spectra of the adhesives almost completely cured under high-moisture conditions suggests the development of more physically entangled networks in the case of urea-derived polymeric structures [64]. These networks, in turn, are likely facilitated by the increased flexibility and heterogeneity of the polymers which result from chain extension during curing in the presence of moisture [65]. Moreover, up until now, crosslinking density has referred exclusively to the covalent urethane and urea bonds formed between the reactive NCO and OH groups. It is expected, however, that hydrogen bonding in these systems will be quite extensive [53, 66, 67]; the excess OH groups of castor oil and the N-H moiety of the urea and urethane groups are proton donating, whilst both the carbonyl (C=O) and ether (CO-O-) moieties of the urea, urethane and ester groups are proton accepting. Thus, every urea can form at least one hydrogen bond more than an analogous urethane group [66]. Furthermore, it is known that the urea hydrogen bonds are stronger than that of the urethane hydrogen bond [67, 68]. Combined, these should result in closer packing of the hydrogen bonded ureas to each other [67], which would in turn account for the increased hardness of the urea-containing adhesives compared to the urethane-only ones. This result also agrees well with the results of the FTIR deconvolution (Figure 6b) in which only hydrogen-bonded urea peaks were observed. Finally, since physical entanglements and the weaker hydrogen bonds reform faster than the covalent ones, this extensive hydrogen bonded network may also account for both the faster relaxation times and the higher flexibilities (as inferred from their lower glass transition temperatures in Section 3.3.2) of the urea-containing adhesives compared to the urethane-only ones.

3.4 Adhesive Properties

Adhesive properties were evaluated via two complementary methods: lap shear and probe tack tests. In the lap shear experiments, the adhesive is cured between two contacts and the resistance to debonding as the two contacts are sheared from each other is captured as the shear stress. In the probe tack experiment, the adhesive performance under short contact times (*i.e.*, pressure sensitive capabilities) is captured as the energy required to separate the substrates shortly after being brought into contact with the already cured adhesive. The former is useful as a measure of long term performance, while the latter is useful for characterizing pressure sensitive adhesive properties. The results are presented in Figures 12a and 12b, respectively.

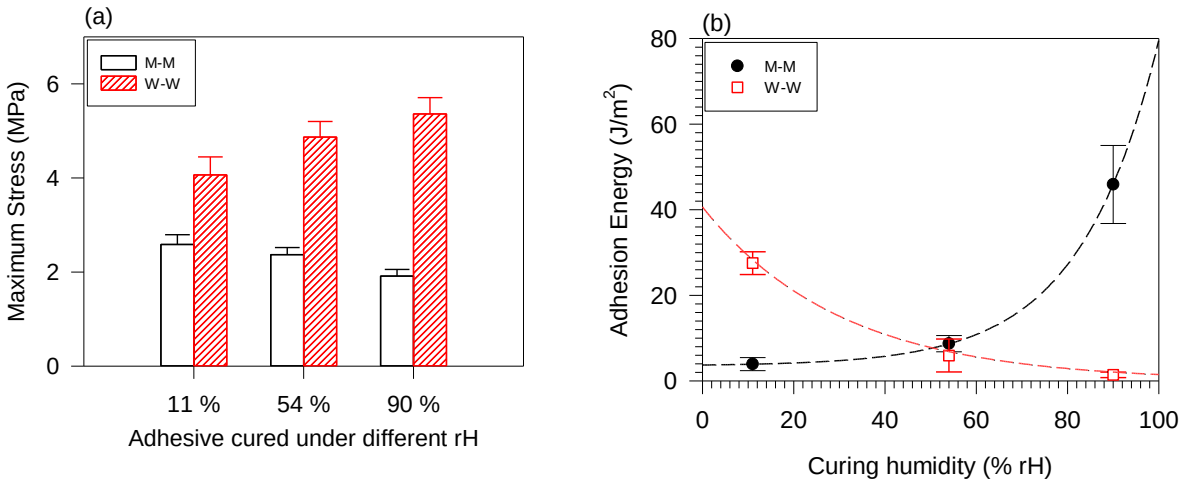

Figure 12: (a) Stress values obtained upon shear debonding of adhesives cured between selected substrates at different humidities (M-M represents the stainless steel metal-metal contacts, and W-W the wood-wood contact). (b) Adhesion energies from tacking experiments with adhesives which were fully cured under different humidity environments and stainless steel or wood contacts.

Figure 12a shows that the shear strengths of the adhesives are greater in wood-wood contact applications compared to metal-metal contact applications. This difference is

expected since, at t_0, the available NCO in the adhesives can form covalent bonds with the OH groups on the lignocellulosic components of the wood substrates, whilst, in the absence of H-active functional groups on metal surfaces, they only form physical bonds between the metal contacts. This difference is further captured in their adhesion failure mechanisms; the adhesives fail cohesively in all of the wood-wood contacts, whilst in the metal-metal contacts they fail by a combination of both cohesive and adhesive failure mechanisms (≈ 50:50%). Of particular note is that these systems present shear strengths which are at least two times higher than those reported in the literature under similar test conditions, inclusive of selected commercial adhesives [20, 23].

In Figure 12a, we can also see that humidity influences the adhesion performance of the two substrates differently. In the wood-wood application, curing at higher humidity results in progressively increased shear strength – despite the lower crosslinking density within the adhesive itself. This might be due to the increased hydrogen bonding facilitated between the OH moieties of the wood surfaces and the polar urea groups of the urea-containing adhesives which complement the already chemically crosslinked interface. Upon shear, these hydrogen bonds can reform faster than the chemical-only bonds which break in the analogous urethane-only systems, resulting in increased resistance to shear, similar to what was observed for the bulk material in the stress and frequency sweep experiments already presented in Section 3.3.3. On the other hand, since H-active groups are absent on the stainless steel surfaces, adhesion between the metal-metal contacts would result from primarily electrostatic interactions between the polar groups on the adhesive - namely urea and urethane - and the metal surface. These interactions, which are significantly lower in strength compared to the covalent bonds formed between the adhesive and the wood substrate, are not sufficient to mitigate the loss of chemical cohesive integrity within the adhesive itself with increasing curing humidity. In addition to this, the harder and more shear-

resistant structure achieved by urea formation can favour the adhesive failure at lower stresses.

Surprisingly, Figure 12b shows that the reverse is true for the fully cured adhesives in tack the experiments; upon complete curing, the moisture-cured adhesives perform exponentially better with the metal-metal contact, whilst the system cured at low humidity performs the best with the wood-wood contact. At close to ambient humidity, the fully cured adhesive performs the same with both metal and wood contacts. Upon increasing humidity, the significantly higher polarity of the urea-moieties on the adhesive surface permits stronger adhesion with the metal substrates in a short-term contact like tacking. It is also likely that the lesser crosslinked and more heterogeneous adhesives (*i.e.*, the urea-containing adhesives) would possess higher energy-dissipating abilities on account of their decreased structural rigidity but, at the same time, higher viscoelastic moduli compared to the more crosslinked urethane-only adhesives, thus contributing to the higher adhesion energy during the tacking experiments [69-72]. On the other hand, the poorer performance of the urea-containing adhesives with wood can be attributed to poor contact between the cured adhesive film and the wood surface. Unlike the metal surface which was smooth, untreated wood surfaces are typically porous and contain many asperities. As presented in the preceding section, the urea-containing adhesive is also the hardest, and thus is least capable of wetting the wood surface sufficiently to create a strong contact line under the conditions of our tacking experiments.

Overall, these results show that as curing agents, these systems are better suited for wood-wood or similar applications in which the formation of strong covalent bonds between the substrate and the adhesive can be facilitated. Furthermore, small improvements in shear performance can be obtained with curing at high humidities. At the same time, when fully cured at increasingly high humidities, these same systems demonstrate the potential to be

used as pressure sensitive adhesives for contacts such as, but not limited to, stainless steel and other metals.

4 Conclusions

To conclude, we have subjected an NCO-terminated castor oil derived urethane adhesive to different curing humidities in order to correlate the expected changes in chemical composition with differences in thermal and mechanical properties and adhesive performance. In systems cured in the absence of moisture, the adhesives were more covalently crosslinked. On account of stronger hydrogen bonds, the urea-containing adhesives - which were obtained upon curing in the presence of moisture - were harder gel-like systems, more resistant to deformation, and recovered faster when subjected to shear deformation compared to the urethane-only adhesive. Expectedly, adhesive performance was better for substrates with which covalent links were possible. In wood-wood contact, curing in the presence of moisture resulted in increased performance due to the strong H-bonds which complimented the already present covalent bonds. On the other hand, adhesive performance with metal contacts decreased when the combined systems were cured at higher humidity because of the lower overall cohesive strength and increased viscoelastic moduli in the urea-containing adhesives, which favours the adhesion failure at lower stresses. This was contrary to the better adhesion performance obtained during tacking experiments with the fully cured urea-containing adhesives and metal contacts, attributed to the increased surface polarity, hardness and the energy dissipating ability of the adhesives when cured in the presence of moisture. Overall, the thermal, mechanical properties and adhesion performance of our model adhesive depended very strongly on the subtle changes in chemical composition which accompanied curing under different humidity environments.

Supporting Information

Supporting Information is provided.

Author Information

Corresponding Author

*J. M. Franco. E-mail: franco@uhu.es

Notes

The authors declare no financial conflict.

Acknowledgements

The authors gratefully acknowledge the financial support of the European Union and Procter and Gamble (EU) for this work, performed under the research project ISSFLOW-FP7-PEOPLE-2013-IAPP-612330.

References

[1] A.L. Lambuth, Adhesives from renewable resources: Historical perspective and wood industry needs, in Adhesives from renewable resources, R.W. Hemingway, A.H. Conner, and S.J. Branham, Editors. 1989, ACS Symposium series-American Chemical Society (USA): Washington, DC. p. 1-10.

[2] B. Nohra, et al., From petrochemical polyurethanes to biobased polyhydroxyurethanes. Macromolecules, 46 (2013) 3771-3792.

[3] A. Gandini, et al., Progress of polymers from renewable resources: furans, vegetable oils, and polysaccharides. Chem. Rev., 116 (2015) 1637-1669.

[4] V. Sharma and P. Kundu, Condensation polymers from natural oils. Prog. Polym. Sci., 33 (2008) 1199-1215.

[5] S. Miao, et al., Vegetable-oil-based polymers as future polymeric biomaterials. Acta Biomater., 10 (2014) 1692-1704.

[6] A. Shirke, B. Dholakiya, and K. Kuperkar, Novel applications of castor oil based polyurethanes: a short review. Polym. Sci., Ser. B, 57 (2015) 292-297.

[7] I. Javni, W. Zhang, and Z.S. Petrović, Effect of different isocyanates on the properties of soy-based polyurethanes. J. Appl. Polym. Sci., 88 (2003) 2912-2916.

[8] Z.S. Petrović, et al., Effect of OH/NCO molar ratio on properties of soy-based polyurethane networks. J. Polym. Environ., 10 (2002) 5-12.

[9] C. Zhang, S.A. Madbouly, and M.R. Kessler, Biobased polyurethanes prepared from different vegetable oils. ACS Appl. Mater. Interfaces, 7 (2015) 1226-1233.
[10] P.K. Pillai, M.C. Floros, and S.S. Narine, Elastomers from Renewable Metathesized Palm Oil Polyols. ACS Sustainable Chem. Eng., 5 (2017) 5793–5799.
[11] J.-M. Raquez, et al., Thermosetting (bio) materials derived from renewable resources: a critical review. Prog. Polym. Sci., 35 (2010) 487-509.
[12] H. Mutlu and M.A. Meier, Castor oil as a renewable resource for the chemical industry. Eur. J. Lipid Sci. Technol., 112 (2010) 10-30.
[13] T. Gurunathan, S. Mohanty, and S.K. Nayak, Isocyanate terminated castor oil-based polyurethane prepolymer: Synthesis and characterization. Prog. Org. Coat., 80 (2015) 39-48.
[14] B.B. Silva, R.M. Santana, and M.M. Forte, A solventless castor oil-based PU adhesive for wood and foam substrates. Int. J. Adhes. Adhes., 30 (2010) 559-565.
[15] P.K. Devi, et al., Urethane-forming reaction kinetics of natural oil polyols versus petroleum-based polyether polyol. Reaction Kinetics, Mechanisms and Catalysis, 119 (2016) 93-106.
[16] K. Liu, et al., Castor oil-based waterborne polyurethanes with tunable properties and excellent biocompatibility. European Journal of Lipid Science and Technology, 118 (2016) 1512-1520.
[17] S. Li, et al., Thermoplastic Polyurethanes Stemming from Castor Oil: Green Synthesis and Their Application in Wood Bonding. Coatings, 7 (2017) 159.
[18] P.N. Moghadam, et al., Preparation of polyurethane wood adhesives by polyols formulated with polyester polyols based on castor oil. International Journal of Adhesion and Adhesives, 68 (2016) 273-282.
[19] L.R. Fonseca, et al. Self-Metathesis of 10-Undecen-1-Ol with Ru-Amine-Based Complex for Preparing the Soft Segment and Chain Extender of Novel Castor Oil-Based Polyurethanes. in Macromolecular Symposia. 2016. Wiley Online Library.
[20] A. Tenorio-Alfonso, M.C. Sánchez, and J.M. Franco, Preparation, characterization and mechanical properties of bio-based polyurethane adhesives from Isocyanate-functionalized cellulose acetate and castor oil for bonding wood. Polymers, 9 (2017) 132.
[21] A.M. Borrero-López, C. Valencia, and J. Franco, Rheology of lignin-based chemical oleogels prepared using diisocyanate crosslinkers: Effect of the diisocyanate and curing kinetics. Eur. Polym. J., 89 (2017) 311-323.
[22] R. Gallego, et al., Gel-like dispersions of HMDI-cross-linked lignocellulosic materials in castor oil: toward completely renewable lubricating grease formulations. ACS Sustainable Chem. Eng., 3 (2015) 2130-2141.
[23] A. Tenorio-Alfonso, et al., Assessing the rheological properties and adhesion performance on different substrates of a novel green polyurethane based on castor oil and cellulose acetate: a comparison with commercial adhesives. International Journal of Adhesion and Adhesives, 82 (2018) 21–26.
[24] S. Fernández-Prieto, J.M. Franco, I. Martinez, L.C. Raghunanan, Adhesives derived from castor oil, European Patent, 2017, application number 17382 599.3.
[25] S. Fernández-Prieto, J.M. Franco, E. Fratini, C. James, I. Martinez, D.G. O'Sullivan, G. Saini, H.D. Santan, J. Smets, R. Vyas, Gels comprising a hydrophobic material, European Patent, 2017, application number 17382484.8.
[26] R. Jayamurugan, et al., Influence of temperature, relative humidity and seasonal variability on ambient air quality in a coastal urban area. International Journal of Atmospheric Sciences, 2013 (2013).
[27] N.R. Canada, Keeping The Heat In, in M144-41/2012E-PDF. 2017: Canada. p. 124.

[28] E. Slatina, et al., Correlation between change in air humidity and the incidence of stroke. Materia socio-medica, 25 (2013) 242.
[29] H. Ni, et al., Effect of catalysts on the reaction of an aliphatic isocyanate and water. J. Polym. Sci., Part A: Polym. Chem., 40 (2002) 1677-1688.
[30] P. Ferreira, et al., Modification of the biopolymer castor oil with free isocyanate groups to be applied as bioadhesive. Int. J. Biol. Macromol., 40 (2007) 144-152.
[31] V. Romanova, et al., Fourier transform Raman and Fourier transform infrared spectra of cross-linked polyurethaneurea films synthesized from solutions. J. Raman Spectrosc., 33 (2002) 769-777.
[32] M. Burrow, et al., Influence of temperature and relative humidity on early bond strengths to dentine. J. Dent., 23 (1995) 41-45.
[33] A.L. Daniel-da-Silva, J.C.M. Bordado, and J.M. Martín-Martínez, Moisture curing kinetics of isocyanate ended urethane quasi-prepolymers monitored by IR spectroscopy and DSC. Journal of applied polymer science, 107 (2008) 700-709.
[34] T.M. Madkour and R.A. Azzam, Use of blowing catalysts for integral skin polyurethane applications in a controlled molecular architectural environment: Synthesis and impact on ultimate physical properties. Journal of Polymer Science Part A: Polymer Chemistry, 40 (2002) 2526-2536.
[35] Z. Ling, et al., In-situ chemical structure analysis of aqueous vinyl polymer solution-isocyanate adhesive in post-cure process by using Fourier transform near infrared spectroscopy. International Journal of Adhesion and Adhesives, 81 (2018) 56-64.
[36] D. Chattopadhyay, B. Sreedhar, and K. Raju, Influence of varying hard segments on the properties of chemically crosslinked moisture-cured polyurethane-urea. Journal of Polymer Science Part B: Polymer Physics, 44 (2006) 102-118.
[37] A.K. Mishra, et al., Thermal and dynamic mechanical characterization of polyurethane–urea–imide coatings. Journal of applied polymer science, 102 (2006) 3158-3167.
[38] D. Ren and C.E. Frazier, Structure–property behavior of moisture-cure polyurethane wood adhesives: Influence of hard segment content. International Journal of Adhesion and Adhesives, 45 (2013) 118-124.
[39] D. Ren and C.E. Frazier, Wood/adhesive interactions and the phase morphology of moisture-cure polyurethane wood adhesives. International Journal of Adhesion and Adhesives, 34 (2012) 55-61.
[40] M. Wen and K. Adamsons, In Situ FTIR Study of Cure Kinetics of Coatings with Controlled Humidity, in Protective Coatings. 2017, Springer. p. 169-193.
[41] A. Wexler and S. Hasegawa, Relative humidity-temperature relationships of some saturated salt solutions in the temperature range 0 to 50 C. J. Res. Natl. Bur. Stand., 53 (1954) 19-26.
[42] S.P. Pinho and E.A. Macedo, Solubility of NaCl, NaBr, and KCl in water, methanol, ethanol, and their mixed solvents. J. Chem. Eng. Data, 50 (2005) 29-32.
[43] L. Greenspan, Humidity fixed points of binary saturated aqueous solutions. Journal of research of the national bureau of standards, 81 (1977) 89-96.
[44] L.H. Chan-Chan, et al., Characterization of model compounds and poly (amide-urea) urethanes based on amino acids by FTIR, NMR and other analytical techniques. Eur. Polym. J., 92 (2017) 27-39.
[45] G. Campanella, et al., On the origin of primary aromatic amines in food packaging materials. Trends Food Sci. Technol., 46 (2015) 137-143.
[46] B.F. d'Arlas, et al., Kinetic and thermodynamic studies of the formation of a polyurethane based on 1, 6-hexamethylene diisocyanate and poly (carbonate-co-ester) diol. Thermochim. Acta, 459 (2007) 94-103.

[47] K. Schwetlick and R. Noack, Kinetics and catalysis of consecutive isocyanate reactions. Formation of carbamates, allophanates and isocyanurates. J. Chem. Soc., Perkin Trans. 2, (1995) 395-402.
[48] S. Zhang, et al., FTIR spectroscopic characterization of polyurethane-urea model hard segments (PUUMHS) based on three diamine chain extenders. Spectrochim. Acta, Part A, 66 (2007) 188-193.
[49] M. Ionescu, Chemistry and technology of polyols for polyurethanes. 2005: iSmithers Rapra Publishing.
[50] F. Dimier, et al., Curing kinetics and chemorheological analysis of polyurethane formation. Polym. Eng. Sci., 44 (2004) 518-527.
[51] L. Moreira, V. Costa, and F.N. da Silva, Effect of moisture content on curing kinetics of agglomerate cork. Mater. Des., 82 (2015) 312-316.
[52] T.N.M. Tuan Ismail, et al., Urethane-forming reaction kinetics and catalysis of model palm olein polyols: quantified impact of primary and secondary hydroxyls. J. Appl. Polym. Sci., 133 (2016).
[53] D. Chattopadhyay, B. Sreedhar, and K. Raju, The phase mixing studies on moisture cured polyurethane-ureas during cure. Polymer, 47 (2006) 3814-3825.
[54] Z. Yang, et al., Polyglycerol-based organic-inorganic hybrid adhesive with high early strength. Mater. Des., 117 (2017) 1-6.
[55] W.W. Nawar, Thermal degradation of lipids. J. Agric. Food Chem., 17 (1969) 18-21.
[56] D. Chattopadhyay and D.C. Webster, Thermal stability and flame retardancy of polyurethanes. Prog. Polym. Sci., 34 (2009) 1068-1133.
[57] G. Montaudo, et al., Mechanism of thermal degradation of polyurethanes. Effect of ammonium polyphosphate. Macromolecules, 17 (1984) 1605-1614.
[58] Y. Zhang, et al., Thermal degradation of polyurethane based on IPDI. J. Anal. Appl. Pyrolysis, 84 (2009) 89-94.
[59] L. Jiao, et al., Thermal degradation characteristics of rigid polyurethane foam and the volatile products analysis with TG-FTIR-MS. Polym. Degrad. Stab., 98 (2013) 2687-2696.
[60] I. Javni, et al., Thermal stability of polyurethanes based on vegetable oils. J. Appl. Polym. Sci., 77 (2000) 1723-1734.
[61] Y. Lu and R.C. Larock, Soybean-oil-based waterborne polyurethane dispersions: effects of polyol functionality and hard segment content on properties. Biomacromolecules, 9 (2008) 3332-3340.
[62] Y. Fourati, et al., A one step route synthesis of polyurethane newtwork from epoxidized rapeseed oil. Prog. Org. Coat., 105 (2017) 48-55.
[63] S.S. Narine, et al., Physical Properties of Polyurethanes Produced from Polyols from Seed Oils: I. Elastomers. J. Am. Oil Chem. Soc., 84 (2007) 55-63.
[64] F.J. Stadler, et al., Linear viscoelastic rheology of moderately entangled telechelic polybutadiene temporary networks. Macromolecules, 42 (2009) 6181-6192.
[65] M. Mazurek-Budzyńska, et al., Poly (carbonate-urea-urethane) networks exhibiting high-strain shape-memory effect. Polym. Adv. Technol., 28 (2017) 1285-1293.
[66] A. Marcos-Fernández, et al., Hydrogen Bonding in Copoly(ether−urea)s and Its Relationship with the Physical Properties. Macromolecules, 30 (1997) 3584-3592.
[67] S. Sami, et al., Understanding the influence of hydrogen bonding and diisocyanate symmetry on the morphology and properties of segmented polyurethanes and polyureas: computational and experimental study. Polymer, 55 (2014) 4563-4576.
[68] L. Born and H. Hespe, On the physical crosslinking of amine-extended polyurethane urea elastomers: A crystallographic analysis of bis-urea from diphenyl methane-4-isocyanate and 1, 4-butane diamine. Colloid Polym. Sci., 263 (1985) 335-341.

[69] T. Wang, et al., Waterborne, nanocomposite pressure-sensitive adhesives with high tack energy, optical transparency, and electrical conductivity. Adv. Mater., 18 (2006) 2730-2734.
[70] B.-m. Zhang Newby and M.K. Chaudhury, Effect of interfacial slippage on viscoelastic adhesion. Langmuir, 13 (1997) 1805-1809.
[71] C. Gay, Stickiness—some fundamentals of adhesion. Integr. Comp. Biol., 42 (2002) 1123-1126.
[72] R. Vendamme and W. Eevers, Sticky degradable bioelastomers. Chem. Mater., 29 (2017) 5353–5363.